Arabian Journal of Chemical and Environmental Research

Vol. 13 Issue 3 (2026) 530–545

Photocatalytic Degradation of Alkali Blue Dye from aqueous solution Using MnO_2 nanoparticles

Ibrahim M. A.[1*], Muhammad A. S.[2] and Umar S.[3]

[1]*Department of Applied Chemistry, Federal University of Technology Babura, Jigawa State, Nigeria,*
[2]*Department of Pure and Industrial Chemistry, Bayero University, Kano, Nigeria,*
[3]*Department of Chemistry, Yobe State University Damaturu, Yobe State, Nigeria,*

Email: *maibrahim.chm@futb.edu.ng, asmuhammed.chm@buk.edu.ng, saniumartafida@gmail.com*

Received: 23 May 2026, Revised 22 July 2026, Accepted xx July 2026

Cited as: *Ibrahim, M. A., Muhammad, A. S. and Umar, S. (2026). Photocatalytic Degradation of Alkali Blue Dye from aqueous solution Using MnO_2 nanoparticles, Arab. J. Chem. Environ. Res. 13(3), 530-545*

Abstract

In this study, MnO_2 nanoparticles was used for the photocatalytic degradation of Alkali Blue (AB). MnO_2 was prepared using co-precipitation method and characterized using XRD, FTIR, SEM, pH_{pzc} and UV-Vis. Parameters that affect degradation efficiency such as contact time, pH, initial dye concentration and catalyst dosage were studied. XRD Results revealed an average crystallite size of 9.14 nm. FTIR showed the appearance of Mn–O stretching vibrations, confirming the formation of the nanoparticle. Band gap energy of 3.76 eV was calculated form the result of UV-Vis. Optimum values of contact time, catalyst dosage, initial dye concentration and pH was found to be 50 minutes, 0.4 g, 10 ppm and 2, respectively. Kinetic result showed that modified freundlich model fits better to the experimental data. UV analysis showed high level of mineralization of the dye and reusability studies showed that the photocatalyst can be reused for more than five successive cycles. Overall MnO_2 can be used an effective photocatalyst for the degradation of AB from wastewater.

Keywords: Alkali Blue, MnO_2, Degradation, Kinetics, Mineralization

**Corresponding author.*
E-mail address: *maibrahim.chm@futb.edu.ng*

1. Introduction

The enormous growth of industrial activities is inevitably linked with a significant rise in the production of pollutants, especially various dyes. Dye manufacturing is nowadays an important sector of the chemical industry. The world production is currently estimated at more than 800,000 tons annually, of which 140,000 tons are lost in wastewater during different stages of their application and manufacturing (Ben Mansour *et al.* 2011). The vast majority of these dyes are non-biodegradable and are thus hazardous

to both humans and the environment (Sharma *et al.* 2018; Akartasse *et al.* 2022; Latifi *et al.* 2025). Dyes are divided into three major classes: (a) disperse or non-ionic dyes; (b) cationic dyes that include all basic dyes; and (c) anionic dyes, which include direct, acidic, and reactive dyes (Fajarwati *et al.* 2020). Alkali Blue is a synthetic anionic dye widely used in textile dyeing, printing, inks, leather finishing, and laboratory staining. It belongs to the triphenylmethane dye family**,** which is known for intense coloration, high molar absorptivity, and structural stability. Since the beginning dye manufacturers have not ceased to make huge efforts in controlling and considerably reducing the volumes and the quantities of dyes released into their effluents. According to the literature survey of researchers' investigations, several management organizations have employed various recycling plans for polluted water that are physically, physiologically, and chemically similar to those found in nature (Raizada *et al.*, 2020). Photocatalysis is the most excellent method for purifying water among the several treatment options. It involves the absorption of light energy to form e^-/h^+ pairs, which subsequently produce redox processes on the surface of the photocatalyst material; these processes occur simultaneously (Ahmed and Haider, 2018). Nanoparticles remove toxic dyes and heavy metals from wastewater through adsorption, ion exchange, and photocatalysis, due to their large specific surface area and the ability to modulate their surface chemistry. Although highly effective, these state-of-the-art nanoadsorbents face challenges related to nanoparticle aggregation (where they clump together, thereby reducing active surface area) and scaling up to industrial levels. To address this, scientists often immobilize the nanoparticles on polymer or membrane supports. Furthermore, most functionalized nanoparticles can be reused for multiple cycles after washing with acidic solutions, which desorb the trapped metals and dyes (R *et al.*, 2020; R *et al.*, 2020; R *et al.*, 2020; R *et al.*, 2020; R *et al.*, 2020;).

Manganese dioxide (MnO_2) is an inorganic metal oxide widely studied for its oxidizing ability, redox activity, and catalytic properties. It appears as a black or dark brown crystalline powder and occurs in nature as the mineral pyrolusite, which is the most important ore of manganese. These structural variations strongly influence its surface area, adsorption capacity, and catalytic efficiency (Tompsett and Islam, 2013). In environmental applications, MnO_2 is extensively used as an adsorbent and catalyst for removing organic pollutants, dyes, and heavy metals from wastewater. Its surface typically carries a negative charge at neutral to alkaline pH, enabling strong electrostatic interactions with cationic species. MnO_2 is also valued for its ability to suppress electron–hole recombination when used as a composite catalyst (Shi *et al.*, 2021).

The objectives of this study are to prepare and characterize MnO_2, study the effect of operational parameters for the photocatalytic degradation of AB dye, and conduct kinetic, mineralization, and reusability studies of the degradation process.

2.0 Materials and Methods

2.1 Synthesis of MnO_2 Nanoparticles

Manganese oxide (MnO_2) nanoparticles were prepared from the salt of manganese chloride through co-precipitation method. The nanoparticles were prepared by mixing manganese chloride dehydrate salt solution and Sodium Hydroxide (NaOH) under constant stirring for 3 hrs. 100 cm^3 solution (0.2 M) of $MnCl_2.2H_2O$ was taken in a titration flask and then 0.4 M NaOH (100 cm^3) solution was added drop by drop at nonstop under continuous stirring until basic pH of the solution was obtained. The mixture was filtered and washed several times with deionized water to eliminate unreacted chemicals. The MnO_2 nanoparticles obtained were dried to constant weight 100 °C (Naz *et al.*, 2023).

2.2 Photocatalytic Experiment

In a typical experiment, 0.2 g of MnO_2 nanoparticle was dispersed in 100cm^3 of the dye solution having a concentration of 10 ppm in a beaker. The above suspension was magnetically stirred for 25 mins in the dark to obtain adsorption-desorption equilibrium to eliminate the error due to any initial adsorption effect. This was then irradiated using UV lamp at 254 nm. A 10 cm^3 aliqout was taken at 10-minutes intervals, centrifuged at 200rpm and filtered prior to absorbance measurement in order to eliminate error due to scattering (Garzali and Muhammad, 2019).

The effect of operational parameters such as time, catalyst dosage, pH and concentration were investigated; the degradation efficiency (D.E %) of each catalyst was evaluated by using equation 1:

$$\mathrm{D.E}\ (\%) = \frac{C_o - C_t}{C_o} \times 100 \qquad 1$$

C_o Represents the initial concentration of each dye solution at time = 0, C_t is the concentration of dye solution by adding the catalyst after some time = t (Garzali and Muhammad, 2019).

2.3 X-ray Diffraction (XRD)

X-ray diffraction measurement was carried out to determine the crystal phase composition and size of the nanocomposite. The measurements were performed on a powder X-ray diffractometer (Malvern PANalytical) equipped with Cu-Kα radiation (λ = 1.5406 Å). The sample was finely ground using an agate mortar and pestle to obtain a homogeneous powder, ensuring uniformity and eliminating preferential orientation effects. The powdered samples were then spread evenly on a glass sample holder or pressed into a flat, smooth surface in a standard sample holder. XRD patterns were recorded in the 2θ range of 10° to 80° at a scanning rate of 2°/min with a step size of 0.02°. The operating voltage and current of the X-ray tube were set at 40 kV and 30 mA, respectively. All measurements were carried out at room temperature under ambient conditions. The diffraction peaks obtained were analysed to identify the characteristic crystalline plane of MnO_2. The average crystallite size (D) will be calculated from

XRD pattern according to the Scherrer equation:

$$D = \frac{K\lambda}{\beta COS\phi} \quad 2$$

where, k is a constant (about 0.9), λ is the wavelength (0.15405 nm), β is the full width at half maximum (FWHM) of the diffraction line and θ is the diffraction angle (Habib *et al.*, 2018)

2.4 Fourier Transform Infrared Spectroscopy (FTIR) Analysis

Fourier Transform Infrared Spectroscopy (FTIR) analysis was carried out to provide information regarding the nature of the functional groups that may participate in the adsorption and degradation process. The analysis was performed using an FTIR spectrometer equipped with an attenuated total reflectance (ATR) accessory. Each powdered sample was dried to eliminate moisture interference and directly placed on the ATR crystal. The samples were firmly pressed against the crystal to ensure optimal contact. FTIR spectra were recorded over a wavenumber range of 4000–500 cm^{-1} with a resolution of 4 cm^{-1}, accumulating 32 scans per sample to improve signal-to-noise ratio.

2.5 Scanning Electron Microscopic (SEM)

SEM analyses were carried out to visualize the surface morphology of the adsorbent/photocatalyst before and after adsorption processes. A thin layer of each sample was mounted onto SEM stubs using double-sided carbon tape. To avoid charging under the electron beam, the samples were coated with a thin layer of gold or platinum using a sputter coater for 60 – 90 seconds. SEM images were acquired at various magnifications (typically 250 × to 50,000×) using an accelerating voltage of 5 – 15 kV.

2.6 UV-Visible Spectroscopy

UV-Visible spectroscopy of the synthesized MnO_2-Np, SnO_2-Np and MnO_2-SnO_2 Nanocomposite was carried out to determine the maximum absorption wavelength of the synthesized nanoparticles and the result was used to calculate the Band Gap Energy. The band gap energy (E_g) of the photocatalyst will be estimated from the absorption spectra using equation 3:

$$E_g = \frac{hc}{\lambda} \quad 3$$

Where E_g = is the band gag energy (eV), h is plank's constant (6.626×10^{-34}Js) and c is the velocity of light (3×10^8 ms^{-1}).

2.7 pH at Point of Zero Charge (pH_{pzc})

The method reported by Ayuba *et al.* (2022) was adopted in the determination of the pH at point of zero charge value of the nanomaterials. 0.2 g of the adsorbent was added to 40 cm^3 of 0.1 M $NaNO_3$ solution in a series of 50 cm^3 centrifuge tubes. The pH was adjusted using 0.1 M HCl and 0.1 M NaOH to obtain the pH range of 2 – 12. The initial pH value of the supernatant in each conical flask was denoted as pH_i.

The contents were shaken using an incubator shaker and allowed to stay for 24 h. after settling the pH values of the supernatant in each tube was measured and denoted as pH_f. The difference between the initial (pH_i) and final (pH_f) was plotted against the initial (pH_i). The point at which the resulting curve intersected with abscissa was pH_{pzc} of the nanomaterial.

3.0 Results and discussion

3.1 X-Ray Diffraction Analysis

Figure 1 represents the XRD patterns of MnO_2 nanoparticle. Crystallinity and crystal phases of the synthesized material were investigated. From the XRD pattern, the diffraction peaks at the 2θ angles of 23.85^0, 37.15^0 and 58.98^0 which corresponds with Braggs planes of (110), (101) and (211). From the XRD analysis, it can be seen that the material is highly crystalline and are found to well match with standard JCDPDS-No. 06–0395. The average crystallite size was calculated to be 9.14nm using Debye Scherer Equation.

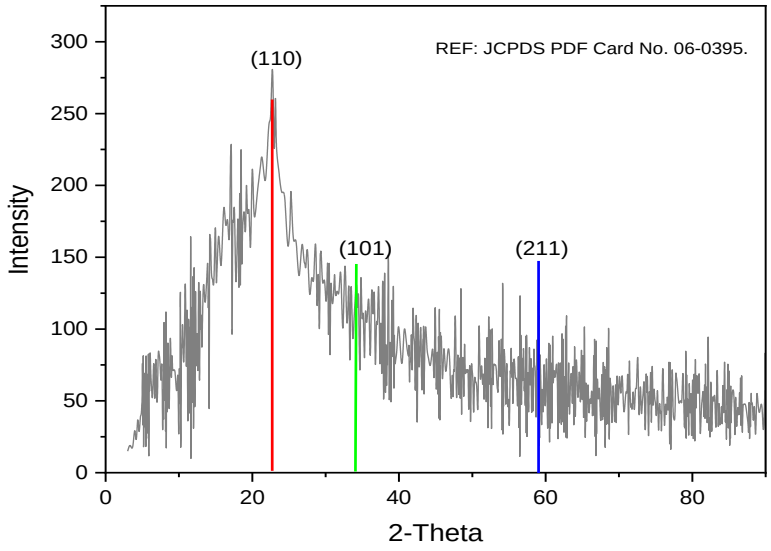

Figure 1: XRD Patterns of MnO_2

3.2 UV-Visible Spectroscopy Studies

Figure 2 and 3 shows the UV-Vis absorption spectrum and Tauc plot of MnO_2 respectively. The optical property of the synthesized MnO_2 is a very important characteristics for the evaluation of their photocatalytic activity. MnO_2 showed a strong absorption peak (λ_{max}) at 330.02 nm in the UV region. This can be attributed to the photo excitation of electron from valence band to conduction band. In this phenomenon, the spectrum obtained was due to optical absorption, which can be analysed to acquire the energy band-gap of the nanomaterials (Yang *et al* 2013). The Band gap energy (E_g) was calculated on the basis of the maximum absorption band of the nanomaterials and was found to be 3.76 eV.

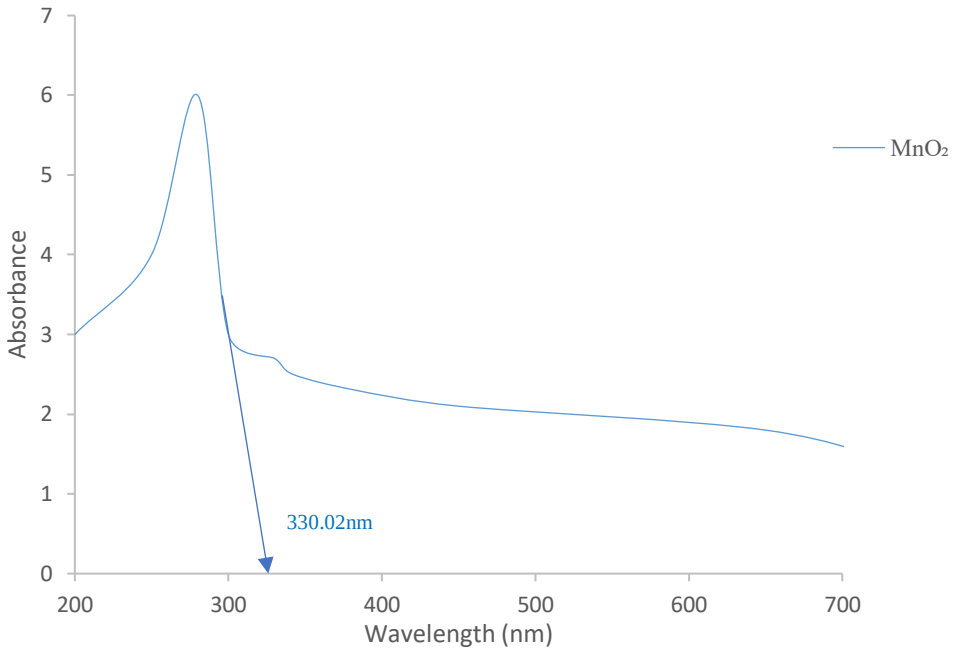

Figure 2: UV-Vis Spectra of MnO_2

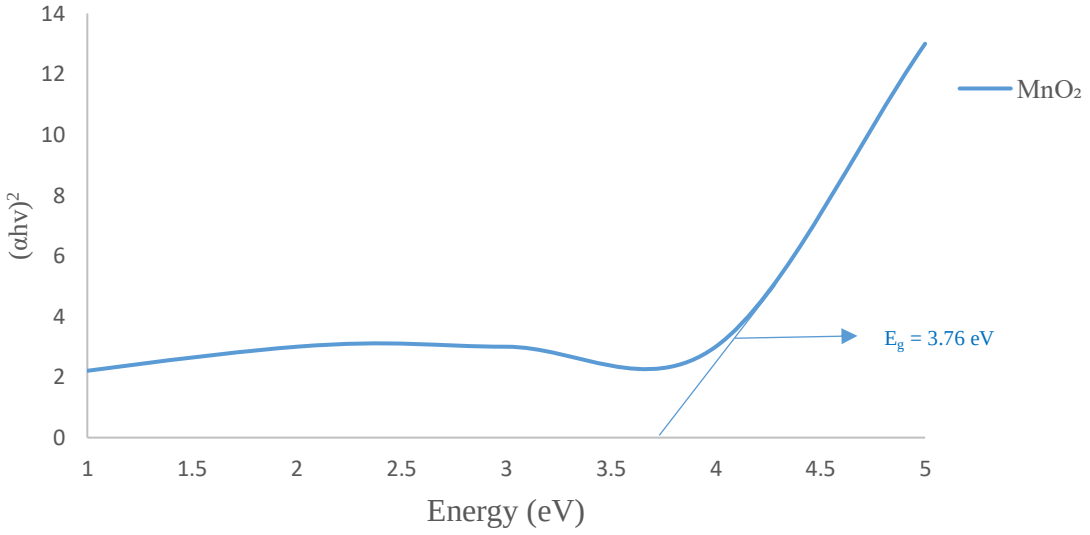

Figure 3: Tauc plot of MnO_2

3.3 pH at Point of Zero Charge (pH_{pzc})

The pH_{pzc} plot of MnO_2, SnO_2 and MnO_2-SnO_2 nanocomposite are displayed in **Figure 4**. pH_{pzc} plays an important role in surface characterization as it determines how easily an adsorbent can adsorb potential harmful ions. This is due to the fact that the adsorbent surface bears net negative charge at pH > pH_{pzc} making the adsorption of cations more favourable. Conversely, at pH < pH_{pzc} values, the adsorbent bears a net positive charge capable of repelling cations (Shoukat *et al.*, 2017). Point of zero charge (pH_{pzc}) values for MnO_2 obtained using salt addition method were found to be 4.5, as presented in **Figure 4**.

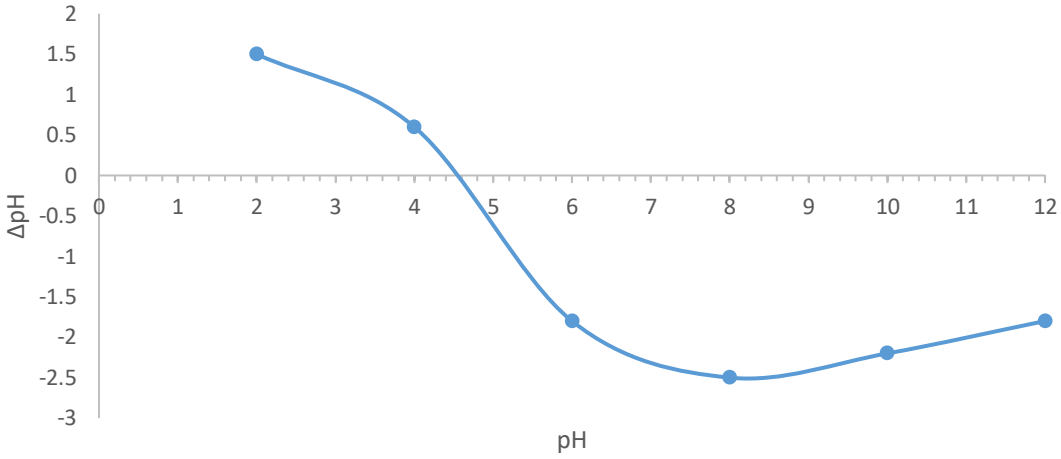

Figure 4: pH_{pzc} Plot for MnO_2

3.4 Fourier Transform Infrared (FTIR) Spectroscopy

Figure 5 shows the FTIR Spectra of MnO_2, before and after adsorption of AB and MY dyes. The spectrum exhibits a broad O–H stretching band at 3363 cm^{-1} and a bending vibration at 1628 cm^{-1}, confirming the presence of surface hydroxyl groups and adsorbed water. The weak peaks at 2191 cm^{-1} and 2242 cm^{-1} can be assigned to C≡C stretching. The weak band at 2922 cm^{-1} is assigned to vibration. The characteristic Mn–O stretching vibrations observed at in the 686 cm^{-1} region verifies the formation of the MnO_2 lattice.

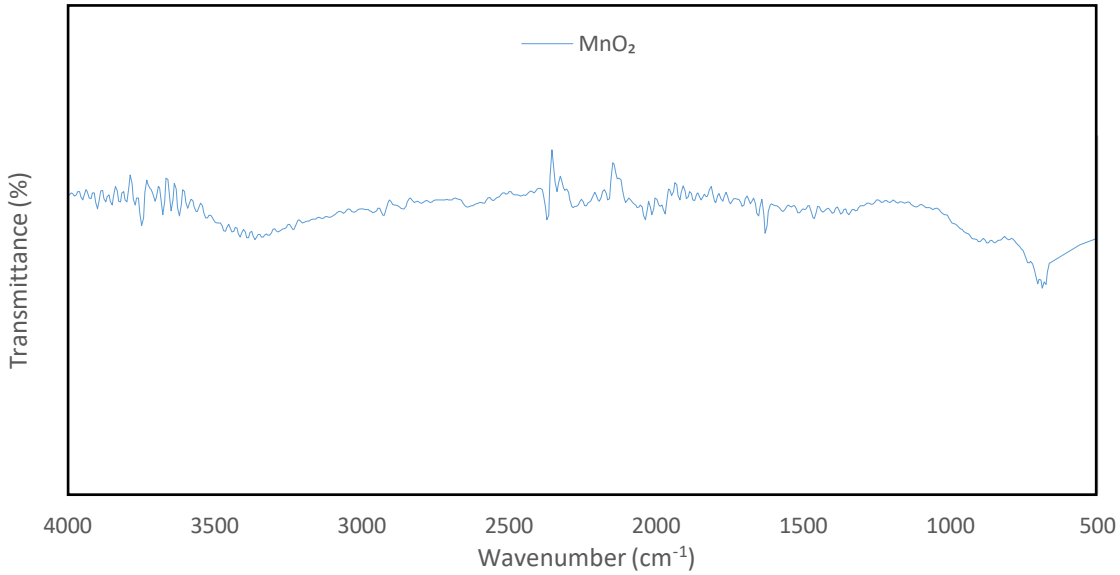

Figure 5: FTIR Spectra of MnO_2

3.5 Scanning Electron Microscopy (SEM)

From **Figure 6**, SEM micrograph of MnO_2 shows irregular, highly agglomerated particles with a rough and porous surface morphology. The presence of surface cracks and intraparticle voids enhances surface area and provides abundant active sites.

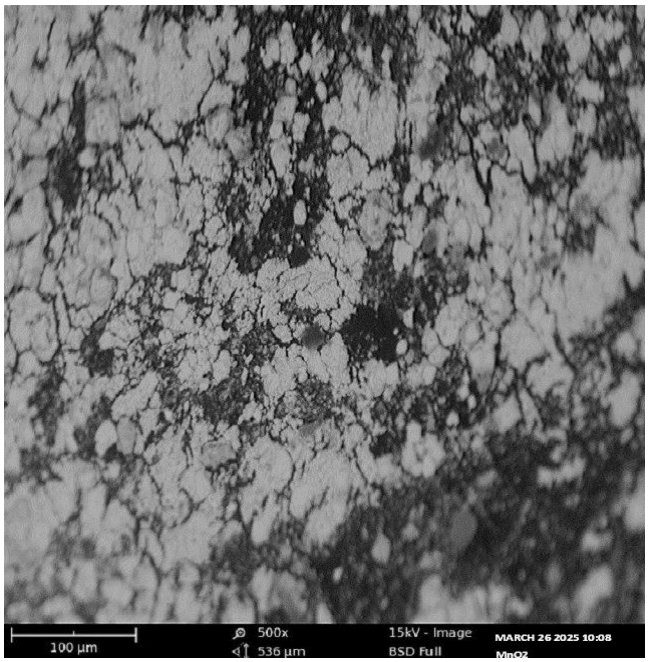

Figure 6: SEM Micrographs of MnO_2

3.6 Impact of Photolysis

The impact of photolysis on the degradation of the AB without the photocatalyst under ultraviolet irradiation (254nm) resulted in a small amount of AB (0.36%) degradation which show that photolysis reaction as shown in **Table 1**. This shows a negligible mineralization of the dyes due to photolysis of the dye using UV light (254 nm).

Table 1: Impact of Photolysis on the degradation of the dyes

Dyes	% Degradation
AB	0.36

3.7 Effect of Experimental Parameters

Effect of experimental Parameters such as Effect of Contact time, Catalyst dosage, Initial dye concentration and pH were carried out.

3.7.1 Effect of Contact Time

Contact time is among the most critical factors for the photocatalytic degradation process. **Figure 7** shows the results of effect of contact time on the photocatalytic degradation of AB dye molecules using MnO_2 which was studied through various time intervals (10–60 min). The experiment involves maintaining consistent reaction conditions while varying irradiation time. The results shows that as the irradiation time increases, the percentage degradation efficiency increases for up to 50minutes for from 40.8 to 73%. There is increase in degradation with increase in time up to 50 minutes followed by slight

decrease in the degradation efficiency. This can be attributed to the increased generation of photo-induced charge carriers on the catalyst surface with prolonged irradiation time (Kalpesh and Vinod, 2019).

Similar trend of result showing fast degradation for a certain period, followed by decrease in degradation was reported by Marwa *et al.*, 2023 during Controlled synthesis of MWCNTs/V_2O_5 nanocomposite by hydrothermal approach for adsorption and photodegradation processes.

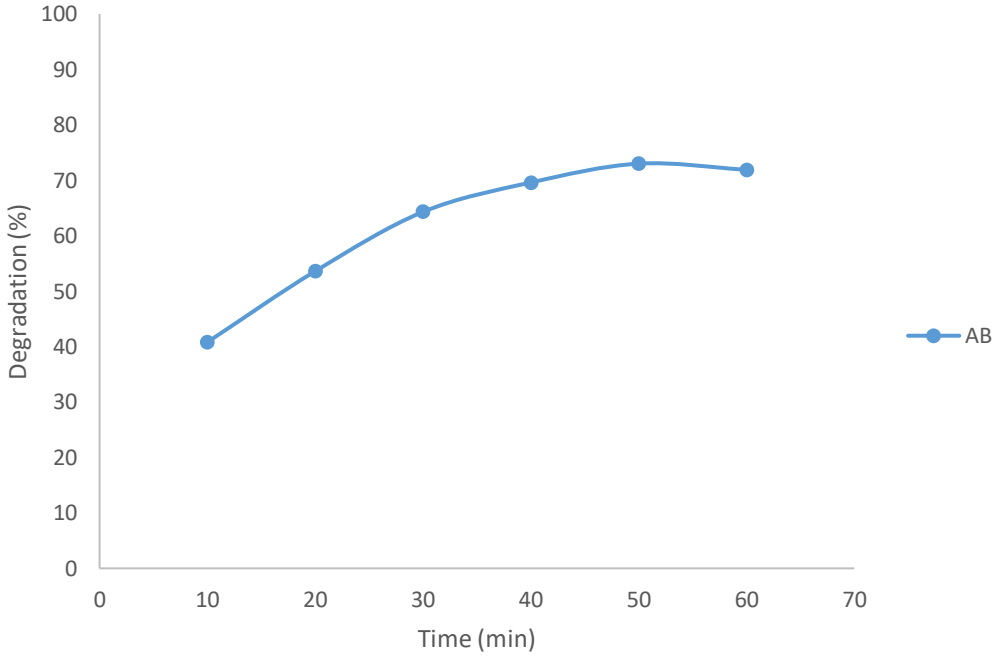

Figure 7: Effect of Contact Time on the Photodegradation of AB Using MnO_2

3.7.2 Effect of Catalyst Dosage

It is known that the photocatalytic degradation rate proportionally depends on the photocatalyst loading in such a way that with increased loading, degradation rate increases until the optimum value. Loading increase has two opposite effects on the efficiency of the photocatalytic process. On one hand, its higher concentrations in the reaction mixture increase the number of active sites for adsorption of pollutants on the photocatalyst surface, which increases the efficiency of degradation. On the other hand, higher photocatalyst loading leads to aggregation of its particles, which increases the dispersion of light from the photocatalyst surface. In addition, aggregation leads to a reduction in the surface area. Therefore, the photocatalyst surface is not available for the generation of $e^- - h^+$ pairs, which can reduce the efficiency of photocatalytic degradation (Méndez-Arriaga *et al.*, 2008).

As illustrated in Figure 8, it shows the influence of MnO_2 dosage on the photocatalytic degradation of AB. The dosage ranges from 0.2 – 1.0g keeping other parameters constant. Based on the obtained results, it can be observed that the degradation efficiency increases with increased photocatalyst loadings up until 0.4 g, and above this value the degradation efficiency slightly drops. This can be

attributed to the accumulation of catalysts in high amounts, which limits the number of active sites at the nanocatalyst's surface (Modirshahla and Behnajady, 2006). Similar results showing increase in degradation efficiency with increase in dosage to its optimum, followed by slight decrease in the degradation efficiency were also reported Fincur *et al.*, 2021 during Environmental Photocatalytic Degradation of Antidepressants with Solar Radiation: Kinetics, Mineralization, and Toxicity.

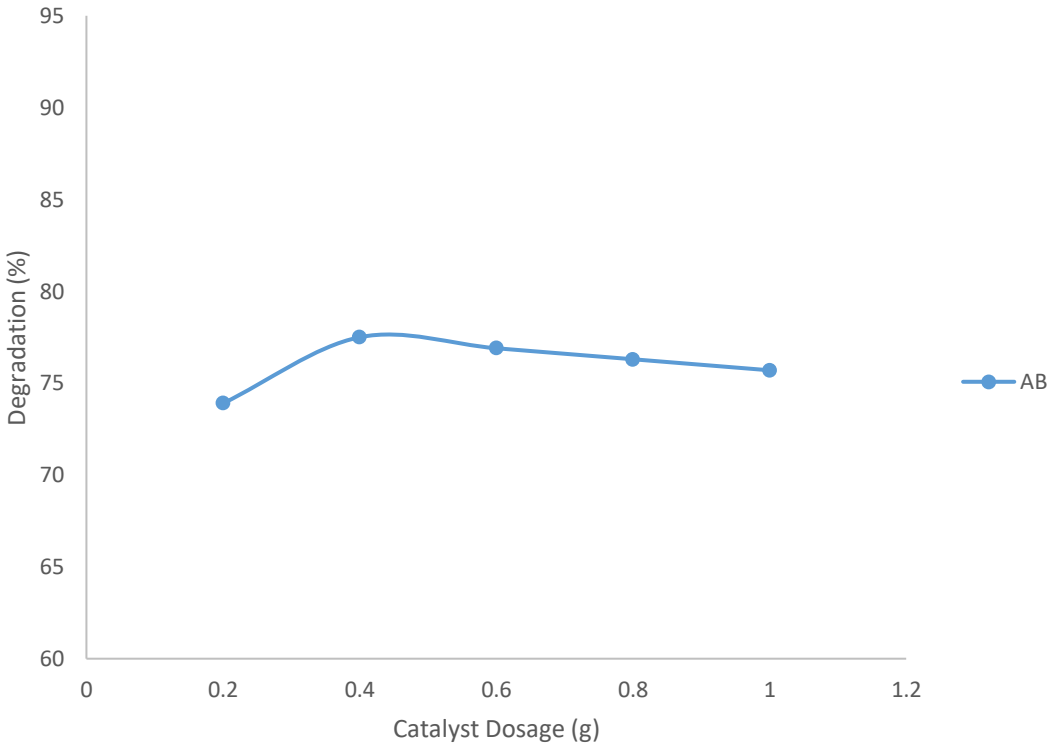

Figure 8: Effect of Catalyst Dosage on the Photodegradation of AB Using MnO_2

3.7.3 Effect of Initial Dye Concentration

The results in **Figure 9** shows the results of effect of Initial dye concentration for AB using MnO_2 photocatalyst. The concentration ranges from 10, 20, 30, 40, 50, 100, 150, 200, 250ppm keeping other parameters constant.

The obtained results disclosed that the photocatalytic performance of the photocatalyst is inversely proportional to the dye concentration at similar conditions, i.e., maximum degradation efficiency was observed at the lowest dye concentration. By raising the concentration from 10 upward, the degradation of the dyes gradually reduce. This is owing to the decreased absorption of light on the photocatalyst surface by raising the dye concentration, which in turn reduces the production of OH• radical ions which play a vital role in the photodegradation process (Priyadharshini *et al.*, 2022).

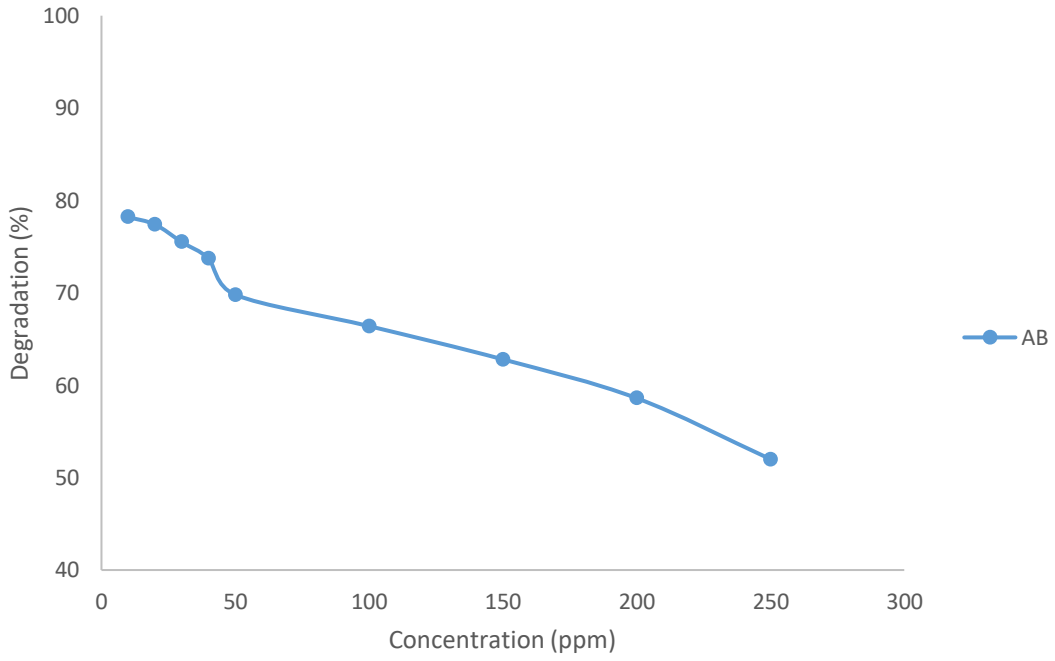

Figure 9: Effect of Initial Dye Concentration on the Photodegradation of AB Using MnO_2

3.7.4 Effect of pH

The role of pH on the photocatalytic degradation of AB using MnO_2 photocatalyst was studied in the pH range of 2 – 12 keeping other parameters constant. The effect of pH on the photocatalytic degradation is dependent on the dyes and the surface charges of the photocatalysts, as the pH of the solution can modify the surface charge of the photocatalyst (Farida *et al.*, 2015).

From **Figure 10**, the experimental result shows that higher degradation of was found to be in acidic conditions. The maximum degradation was obtained at pH 2. This may be attributed to the electrostatic interactions between the positive catalyst surface and dye anions leading to strong adsorption of the dyes on the photocatalyst. The degradation efficiency decreases after the optimum pH value due to the change in the surface properties of the photocatalyst. At higher or lower pH values, the photocatalyst surface can be covered with other species, such as hydroxide ions or carbonate ions, which can inhibit the photocatalytic reaction by reducing the availability of active sites for dye molecules adsorption and oxidation (Maimuna and Abdulfatah, 2022). Similar behavior has also been reported by Krishnan *et al.* 2021 during the effect of pH on the photocatalytic degradation of cationic and anionic dyes using polyazomethine/ZnO and polyazomethine/TiO_2 nanocomposites.

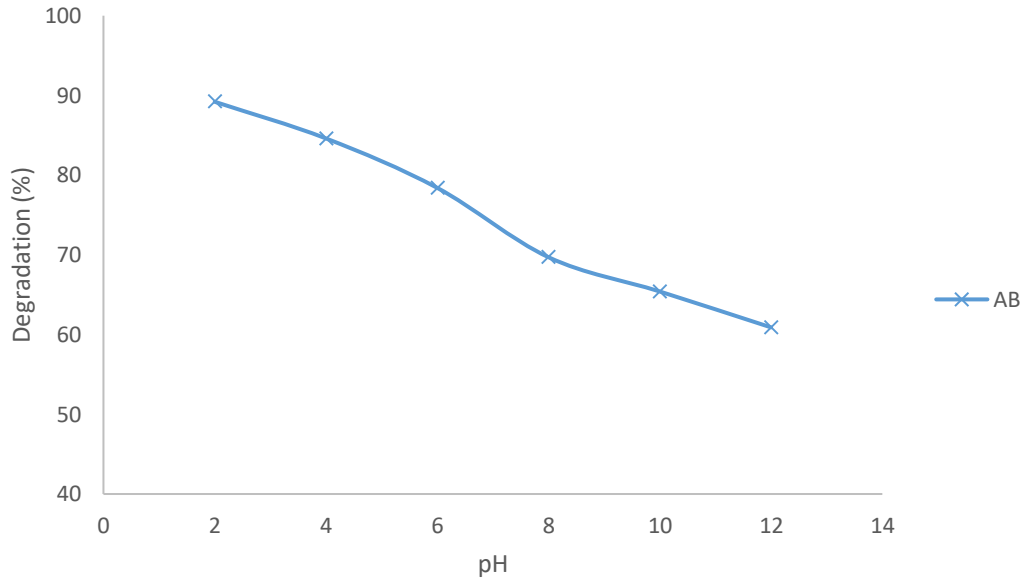

Figure 10: Effect of pH on the Photodegradation of AB Using MnO_2

3.8 Kinetics Study of the Photocatalytic Degradation Process

The photocatalytic degradation of AB dye using MnO_2 under UV light irradiation was investigated to determine the kinetics of the process. The experimental data were fitted into four different kinetics models namely the Langmuir-Hinshelwood model, Pseudo First order, Pseudo Second Order and Modified Freundlich Models, to determine rate of photodegradation of the dyes. The result as presented in **Table 2** shows that Modified Freundlich Model provided a better fit for the experimental data with higher R^2 values compared the other models. The Modified Freundlich model describes heterogeneous diffusion from the flat surface to the solvent using a composition gradient or through molecular ion exchange. This suggests that the system is adsorption-desorption controlled and the photocatalytic photodegradation of the dye molecules are occurring on the photocatalyst surface before leaving (desorption) the surface patches (Rahman *et al.* 2012). This shows that Modified Freundlich Model best fits the data, suggesting that photocatalytic degradation process is potentially effective for the degradation of the dyes.

Table 2: Kinetic Studies for the Photocatalytic Degradation of MnO_2, SnO_2 & MnO_2/SnO_2

Photocatalyst	Dyes	L-H Model		PFO		PSO		MFM	
		Parameters							
		k	R^2	k	R^2	K	R^2	k	R^2
MnO_2	AB	0.376	0.9742	0.3473	0.901	0.5366	0.9849	0.7544	0.9905

3.9 Mineralization of the Dye

The mineralization of AB was evaluated by using UV Analysis. The UV-Analysis of the photodegradation experiments was carried out by scanning the dye solution before and after degradation under UV-Vis irradiation. From **Figure 11**, the solution showed a very high decrease in absorption bands in the presence of the photocatalysts. This indicates high level of mineralization of the dyes using the photocatalysts. This experimental approach involving the dye could be of value in the depollution of real wastewater, using a non-toxic photocatalyst.

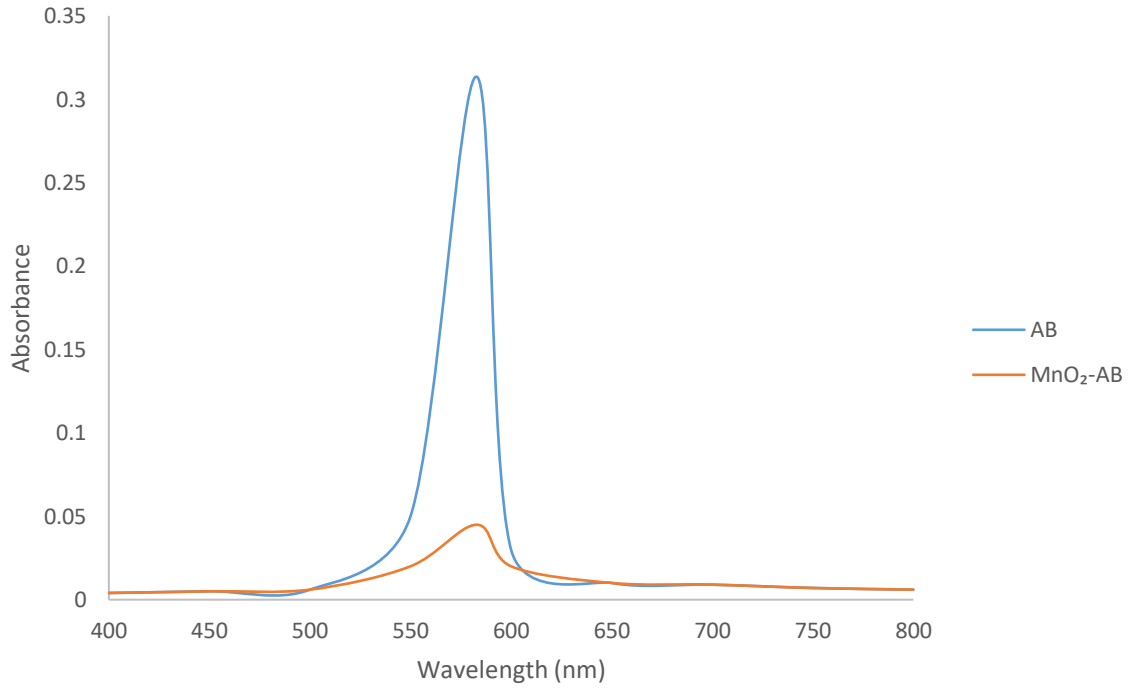

Figure 11: UV-Vis Absorption before and after Photocatalytic Degradation of AB

3.10 Reusability of the Photocatalysts

The reusability efficiency of the photocatalyst had significant impact on the removal process, hence making the application of the materials more economical. In this research the photocatalyst were regenerated by centrifuging in water and ethanol solutions (trice each) for complete cleaning of the catalyst. Then they were dried at 80 ^{o}C for 10 hours and reused for another cycle keeping the concentration of the dyes and photocatalyst constant. The degradation efficiency of AB decreases from the first cycle to the fifth cycle as seen in **Figure 12**. This can be due to loss of mass during the pre-treatment after each cycle. The results shows that the efficiency of the recycled photocatalysts decreased to a little extent and the recycled catalyst was found to be quite efficient for the removal of dyes after reuse.

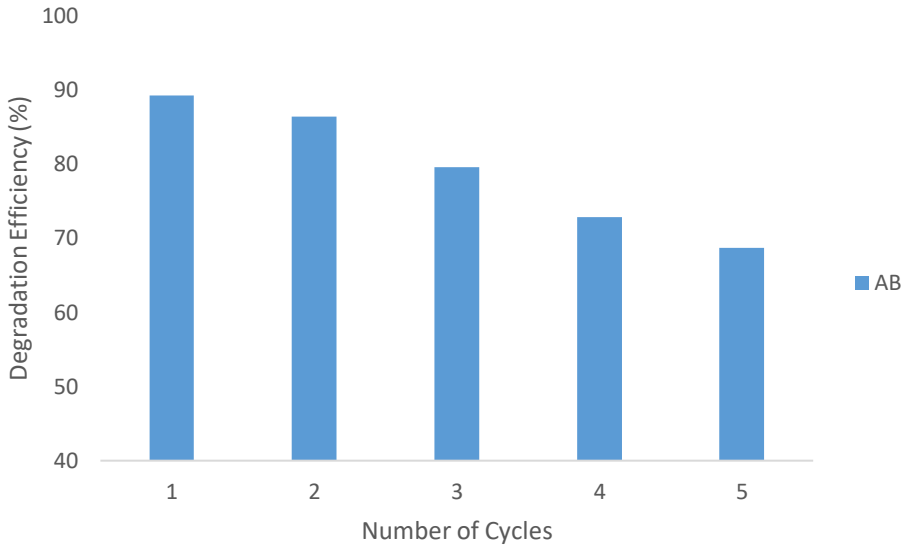

Figure 12: Degradation Efficiency of AB for Reuse with MnO_2 after Five Cycles

Conclusion

Manganese dioxide nanoparticle was successfully synthesized using co-precipitation method. The obtained nanoparticle exhibit an average crystallite size of 9.14 nm, band gap energy of 3.76 eV and pH_{pzc} of 4.5. MnO_2 was employed as a photocatalyst for the degradation of Alkali Blue dye. The degradation performance was investigated by analysing the influence of parameters (time, concentration, dosage and pH). After kinetic evaluation, modified freundlich model was found to represent the data better. Reusability studies showed that the photocatalyst can be efficiently reused even after five successive cycles. In light of the above, MnO_2 can be used as an effective photocatalyst for degradation of AB dye from wastewater.

Conflict of Interest

The authors declare that the research was conducted in the absence of any commercial or financial relationships that could be construed as a potential conflict of interest.

References

Abouri, M., Benzaouak, A., Elouardi, M. *et al.* (2025). Enhanced photocatalytic degradation of Rhodamine B using polyaniline-coated $XTiO_3$(X = Co, Ni) nanocomposites. *Sci Rep* 15, 3595,https://doi.org/10.1038/s41598-024-83610-1

Ahmed, S. N., and Haider, W. (2018). Heterogeneous photocatalysis and its potential applications in water and wastewater treatment: A review. *Nanotechnology*, 29, 342001.

Akartasse N., Azzaoui K., Mejdoubi E., Hammouti B., Elansari L.L., Abou-salama M., Aaddouz M., Sabbahi R., Rhazi L. and Siaj M. (2022), Environmental-Friendly Adsorbent Composite Based

on Hydroxyapatite/Hydroxypropyl Methyl-Cellulose for Removal of Cationic Dyes from an Aqueous Solution, *Polymers*, 14(11), 2147; https://doi.org/10.3390/polym14112147

Ayuba, A. M., Hamza, U., Shurahabil, I. B. and Abdulmumini, H. (2022). Adsorption of Malachite Green Dye using carbonized water Lily Leaves: Kinetics, equilibrium and Thermodynamics studies. *Umaru Musa Yaradua University Scientifica.* 1(1), 91 – 102.

Ben Mansour, H., Boughzala, O., Dridi, D., Barillier, D., Chekir-Ghedira, L. and Mosrati, R. (2011). Les colorants textiles sources de contamination de l'eau : criblage de la toxicité et des méthodes de traitement. Revue des sciences de l'eau / *J Water Sci* 24, 209–238.

Fajarwati, F.I., Yandini, N. Y., Anugrahwati, M. and Setyawati, A. (2020). Adsorption study of methylene blue and methyl orange using green shell (Perna viridis). EKSAKTA *J Sci Data Anal* 1, 92–97

Farida, M. S. E., El Dar Hamed, M., Ibrahim-Heba, A.B., Farag, M., Wahab, Z.A. and Shalabi, M.E.H. (2015). Using Bentonite carbon composite material for adsorption of Bromocresol purple and Methylene blue. *International Journal of Science and Engineering Research,* 6(10), 1-9

Fincur, N., Šojic Merkulov D., Putnik P., Despotovic V., Banic N., Lazarevic M., Cetojevic-Simin D., Agbaba, J., Abramovic, B. (2021). Environmental Photocatalytic Degradation of Antidepressants with Solar Radiation: Kinetics, Mineralization, and Toxicity. *Nanomaterials*, 11, 632.

Garzali, F. A. and Muhammad, A. S. (2019). Degradation of Methyl Red Using Cd-Sb/C Layered Double Hydroxide Catalyst under Visible Light. *Chemsearch Journal,* 10(2), 123-129.

Habib, N. R., Taddesse, A. M., and Temesgen, A., (2018). Synthesis, Characterization and Photocatalytic Activity of $Mn_2O_3/Al_2O_3/Fe_2O_3$ Nanocomposite for Degradation of Malachite Green. *Bull. Chem. Soc. Ethiop.*, 32(1), 101 – 109.

Kalpesh, A.I., and Vinod S.S. (2019). Photodegradation of Methylene Blue using ZnO and 2% Fe-ZnO Semiconductor Nanomaterials Synthesized by Sol-gel Method: A Comparative Study. *SN Applied Sciences*, 1, 1247.

Krishnan, S., Jaiganesh, P. S., Karunakaran, A., Kumarasamy, K. and Mei-Ching Lin (2021). The effect of pH on the photocatalytic degradation of cationic and anionic dyes using polyazomethine/ZnO and polyazomethine/TiO_2 nanocomposites. *International Journal of Applied Science and Engineering.* 18(5), 2020247

Latifi S., Saoiabi S., Alanazi M. M., Boukra O., Krime A., El Hammari L., Azzaoui K., Hammouti B., Hanbali G., Jodeh S., Saoiabi A., *et al*. (2025), Low-Cost Titania-Hydroxyapatite (TiHAp) nanocomposites were synthesized for removal of Methylene blue under Solar and UV irradiation, *Next Materials*, 8, 100859, https://doi.org/10.1016/j.nxmate.2025.100859

Maimuna, U. Z., and Abdulfatah, S. M., (2022). Synthesis, Characterization and Photocatalytic Activity of Eco-friendly ZnCr/C-LDH Nanocatalyst. *Arid Zone Journal of Basic and Applied Research*, 1(4), 25 – 35.

Marwa, H. A., Elsehly, E. M., Mohamed, E. and EL-Maghrabya, E. M. (2023). Controlled synthesis of MWCNTs/V_2O_5 nanocomposite by hydrothermal approach for adsorption and photodegradation processes. *Water Science & Technology*, 88(2), 392.

Méndez-Arriaga, F., Esplugas, S. and Giménez, J. (2008). Photocatalytic degradation of non-steroidal anti-inflammatory drugs with TiO2 and simulated solar irradiation. *Water Res.*, 42, 585–594.

Modirshahla, N. and Behnajady, M. A. (2006). Photooxidative degradation of Malachite Green (MG) by UV/H_2O_2: Influence of operational parameters and kinetic modeling, *Dyes Pigm.* 70, 54-59.

Naz, F., Nabi, G. A. K., Nawaz, A., Sajid Ali, S., and Siddique, M. (2023). A Novel Approach

for the Photocatalytic Degradation of Binary Dyes Mixture Using SnO2 Nanoparticles as a Catalyst. *Journal of Cluster Science*, 34, 2047 – 2066.

Priyadharshini, S.S., Shubha, J.P., Shivalingappa, J., Adil, S.F., Kuniyil, M., Hatshan, M.R., Shaik, B. and Kavalli, K. (2022). Photocatalytic Degradation of Methylene Blue and Metanil Yellow Dyes Using Green Synthesized Zinc Oxide (ZnO) Nanocrystals. *Crystals*, 12, 22.

Rahman, M. M., Choudhury, F.A., Hossain, M.D., Chowdhury, M. N. I., Mohsin, S., Hasan, M., Uddin, M. F. and Sarker, N. C. (2012). A Comparative study on photocatalytic degradation of industrial dyes using modified commercial and synthesized TiO_2 photocatalysts. *Journal of Chemical Engineering*, 27(2), 65-71.

Raizada, P., Sudhaik, A., Patial, S., Hasija, V., Khan, A. A. P., Singh, P., Gautam, S., Kaur, M., and Nguyen, V. H. (2020). Engineering nanostructures of CuO-based photocatalysts for water treatment: Current progress and future challenges. *Arab. J. Chem.*, 13, 8424–8457.

Sharma, B., Dangi, A. K. and Shukla, P. (2018). Contemporary enzyme based technologies for bioremediation: a review. *J Environ Manag* 210, 10–22

Shi, W., Lee, W. S. V. and Xue J. (2021). "Recent Development of Mn-based Oxides as Zinc-Ion Battery Cathode". *Chem. Sus. Chem*. **14** (7): 1634 1658. doi:10.1002/cssc.202002493. ISSN 1864-5631.

Shoukat, S., Bhatti, H. N. and Iqbal, M. (2017). Mango stone biocomposite preparation and application for crystal violet adsorption: *Micro porous and Mesoporous Materials.* 239, 180 – 189.

Tompsett, D. A., and Islam, M. S. (2013). Electrochemistry of Hollandite α-MnO: Li-Ion and Na-Ion Insertion and Li Incorporation. *Chemistry of Materials*, 25 (12), 2515–2526. CiteSeerX 10.1.1.728.3867. doi:10.1021/cm400864n.

Yang, Y., Zhang, Z. C., Wang, P. P., Zhang, J. C., Nosheen, F., Zhuang, J. and Wang, X. (2013). Hierarchial MnO_2/SnO_2 heterostructures for a novel free-standing ternary thermite membrane. *Inorg. Chem.* 52 (16), 9449–9455.